Available online at www.sciencedirect.com
ScienceDirect
Computers and Structures 85 (2007) 866–878
Computers & Structures
www.elsevier.com/locate/compstruc

Modeling physical uncertainties in dynamic stall induced fluid–structure interaction of turbine blades using arbitrary polynomial chaos

Jeroen A.S. Witteveen, Sunetra Sarkar *, Hester Bijl

Faculty of Aerospace Engineering, Delft University of Technology, Kluyverweg 1, 2629 HS Delft, The Netherlands

Received 31 May 2006; accepted 2 January 2007
Available online 20 February 2007

Abstract

A nonlinear dynamic problem of stall induced flutter oscillation subject to physical uncertainties is analyzed using arbitrary polynomial chaos. A single-degree-of-freedom stall flutter model with torsional oscillation is considered subject to nonlinear aerodynamic loads in the dynamic stall regime and nonlinear structural stiffness. The analysis of the deterministic aeroelastic response demonstrated that the problem is sensitive to variations in structural natural frequency and structural nonlinearity. The effect of uncertainties in these parameters is studied. Arbitrary polynomial chaos is employed in which appropriate expansion polynomials are constructed based on the statistical moments of the uncertain input. The arbitrary polynomial chaos results are compared with Monte Carlo simulations.

Keywords: Dynamic stall; Stall flutter; Structural nonlinearity; Uncertainty quantification; Polynomial chaos expansion; Arbitrary uncertainties

1. Introduction

Aeroelastic stability remains an important concern for the design of wind turbine rotors, more so with the use of increasingly flexible blades. Increased flexibility sometimes brings in complex oscillation modes which could be potentially dangerous to the structure [1,2]. Moreover, wind turbine rotors often have to operate at large angles of attack, past the stall angle of the profile, i.e., in the dynamic stall regime. The resulting flow is largely separated and viscous effects are important. The physical process of dynamic stall involves growth and evolution of the leading edge vortex structure and its subsequent shedding from the body into the near wake, all of which have significant influence on the aerodynamic loads. This paper presents an algorithm which can be used to investigate the stall induced oscillation of a two-dimensional profile when one or more system parameters are varied randomly.

1.1. Aeroelasticity and stall flutter

One of the interesting problems in aeroelasticity is the study of stability of a structure in wind. Flutter is a dynamic aeroelastic instability of a structure subjected to aerodynamics forces. Classical flutter involves interaction of vibration modes to transfer energy to and from the vibrating systems. Many researchers have investigated linear and nonlinear flutter problems using analytical methods such as Galerkin approach, direct integration, harmonic balance method, perturbation methods, etc. [3]. A traditional approach to a flutter problem (both experimental and numerical) uses bending-torsion or bending-torsion-edgewise modes of a blade profile and have been widely used in the aeroelastic community [4–7]. Thus, an infinite dimensional problem is replaced by a two or three degrees-of-freedom system. This will not give an exact prediction of the critical airspeed, etc., but will indicate the

* Corresponding author. Tel.: +31 152785169; fax: +31 152787077.
E-mail address: S.Sarkar@tudelft.nl (S. Sarkar).

0045-7949/$ - see front matter
doi:10.1016/j.compstruc.2007.01.004

type of instabilities as a function of the systems parameters that can occur in the real system. Thus, over the years such analyses have been helpful in understanding the real aeroelastic systems [5]. The aerodynamic models used in such studies vary from simple incompressible, inviscid theory to complex Navier–Stokes models. In this paper, a stall flutter oscillation problem is investigated under the purview of the above approaches. The aerodynamics in stall flutter is more complex than traditional flutter. The mode of oscillation is mainly in the torsional direction, unlike the traditional bending-torsion case [3,4].

The stall flutter model considered here is commensurate with the common engineering approach towards aeroelastic problems in aircraft and rotors [6–9]. Such models give enough physical insight to the real life problem and yet allow one to keep the computational efforts less involved. The blade model consists of a two-dimensional symmetric airfoil with a torsional elasticity [10]. In this paper, we also add a cubic stiffness in the structural model [8,11]. Lee et al. [8] point out that a blade section which is being twisted is likely to behave as a cubic stiffness or hardening spring, i.e., it will become stiffer as the twist increases. Moreover, parabolic and cubic stiffness terms could also model some types of control mechanisms that may be present [5,7,11]. Dowell et al. [12] and O'Neil and Strganac [13] have listed several literature which validate and study cubic stiffness nonlinearity in aeroelastic structures. For a detailed discussion on discretization of structural stiffness we refer to Bathe [14].

The blade structure is subjected to aerodynamic moment at the dynamic stall regime. The aerodynamic moment during dynamic stall are calculated using an engineering dynamic stall model developed by Onera [15,16]. This stall model approximates the loads well and is computationally much less expensive than a full viscous solver [17]. Beedy et al. [18] compare the aerodynamic loads by Onera with experimental data and they match quite well. The aerodynamic moment of the Onera model is given by a set of ordinary differential equations. These are combined with the structural equations of motion to derive the set of the nonlinear governing equations of the aeroelastic system. A preliminary deterministic study of the unforced aeroelastic system showed strong influence of nondimensional parameters like nondimensional speed (function of wind speed and torsional frequency) and structural nonlinearity on the Hopf bifurcation behavior of the system [19].

1.2. Uncertainty analysis

In practice the physical parameters in the dynamic stall model are not exactly known or they can be subject to inherent physical variability. Since the system is sensitive to input variations, the uncertainty in the parameters can have a strong influence on the dynamic properties of the blade. Therefore there is a need to study the effect of uncertainties in the system parameters on the bifurcation behavior and the limit cycle oscillation of the stall flutter system. However, this can be computationally quite expensive.

Recently, enough computer power has become available to counteract the increase in computational costs for performing an uncertainty quantification compared to a deterministic simulation. Numerous methods have been used in recent years to quantify physical uncertainties in a variety of computational problems like the Monte Carlo approach, the perturbation method [20] and polynomial chaos expansions [21].

The Monte Carlo approach is based on solving the deterministic problem multiple times for randomly chosen parameter values. Due to the slow convergence rate of standard Monte Carlo usually many samples are required. If solving the deterministic problem is already computationally intensive, the computational costs of a Monte Carlo simulation can become impractical. A fast method for obtaining uncertainty information in terms of the first and second statistical moments is the perturbation method [20]. Here the statistical moments of the output are determined by expanding the stochastic quantities around their mean via a Taylor series expansion. The application of the perturbation method is, however, limited to small perturbations.

The polynomial chaos expansion [21] has proven to be a successful approach to solve uncertainty quantification problems. It is an expansion of orthogonal polynomials in terms of random variables to approximate the full uncertainty distribution of the output. The polynomial chaos expansion coefficients are solved by using a Galerkin stochastic finite element approach. The original homogeneous polynomial chaos expansion [21] is based on the homogeneous chaos theory of Wiener [22,23]. It employs Hermite polynomials and Gaussian random variables. The homogeneous polynomial chaos expansion can approximate any functional in $L_2(C)$ and converges in the $L_2(C)$ sense [24]. Since the Hermite polynomials are orthogonal with respect to the Gaussian measure, the homogeneous polynomial chaos can achieve optimal exponential convergence for Gaussian inputs [25].

The exponential convergence of the polynomial chaos expansion has been extended to several other types of commonly used probability distributions in the generalized polynomial chaos by Xiu and Karniadakis [26]. In the generalized polynomial chaos several classical polynomials of the Askey scheme of hypergeometric orthogonal polynomials are employed, which are orthogonal with respect to other probability distributions such as the gamma and beta distributions. A multi-element version of the generalized polynomial chaos has been developed by Wan and Karniadakis [27] to improve the resolution of singularities in the random space and long-term integration. Generalized polynomial chaos and multi-element generalized polynomial chaos have been applied by Karniadakis and co-workers to for example flow problems and fluid–structure interaction problems in [28–31].

The correspondence of the probability measure in the orthogonality relation of the basis polynomials and the

exponential convergence has been extended to arbitrary input distributions in [27,32]. The arbitrary polynomial chaos is a combination of polynomial chaos and an orthogonalization method. Orthogonalization is employed to construct a polynomial chaos basis orthogonal with respect to the input uncertainty distribution. A more detailed discussion on this has been provided later in this paper.

1.3. Aeroelastic analysis and uncertainty

Probabilistic study of aeroelasticity is one of the recent research trends. Here some of the important contributions in this category are revisited. There are two major issues in aeroelastic analysis: structures and aerodynamics. Most of the earlier works mainly focus on the stability of linear structures under the influence of aerodynamic gust loading. Some of the earlier researches have found mention in [3,33].

We find mention of one of the earlier uncertainty works with a bending-torsion flutter model in an unpublished report by Poirion [34,35]. The author has used a first-order perturbation method to predict the flutter probability with uncertainty considered in structural mass and stiffness. Pettit [35,36] has outlined the influence of uncertainty in various aspects of aeroelastic design, both static and dynamic which are integral parts of an airframe design. In these reviews, the author has concluded that small variations in the system parameters, external loads and boundary conditions can significantly modify the aeroelastic system response. Poirion [37] has investigated the problem of nonlinear random oscillations with application to aeroservoelastic systems. Here the author has outlined the simulation techniques for Gaussian and non-Gaussian random processes and random delay modeling of control systems. Borglund [38] has considered a frequency domain linear flutter model using Reissner's aerodynamic model. This model uses a truncated Fourier series approximation for the aerodynamic loads. The first few Fourier coefficients of this model have been assumed to be uncertain and the flutter stability has been investigated using a standard μ-analysis. Pettit and Beran [39,40] have presented a Wiener–Hermite chaos representation of bending-torsion flutter model and pointed out the problem of energy loss at large time intervals. In order to understand this energy loss, they have investigated a test problem of sinusoidal oscillation with random frequency. They have shown that at large time intervals, the nonlinearity of the problem increases with the random variable and that a polynomial chaos expansion can have difficulty representing such a response. To improve the performance of chaos expansions in long-term integration, Pettit and Beran [39] have applied Wiener–Haar expansions, developed by Le Maître et al. [41], to time dependent problems. Millman et al. [42] have proposed Fourier chaos to better approximate the stochastic response of aeroelastic systems. Pettit and Gandhi [43] have presented a reliability based weight optimization of a wing model for gust response and aileron effectiveness. The structure is modeled with random thickness and material properties and the aerodynamic model assumes a linear unsteady flow. An improved aeroelastic performance is predicted after redistributing the structural mass using the optimizer routine.

Various studies have focused on the problem of panel flutter and its sensitivity to uncertain system parameters, mostly structural parameters. In one of the earlier works, Liaw and Yang [44] have considered flutter of laminated plates and shells with uncertainties in various structural and geometric parameters. They have used a second moment perturbation based stochastic finite element model. A second moment approach restricted the calculation of the output variability to the second moment also. Ibrahim et al. [45] have also considered a panel flutter problem under random and deterministic in-plane loading and random pressure differential. Effects of boundary condition relaxation and system nonlinearity on the system response have been studied. Choi and Namachchivaya [46] have considered a nonlinear problem of panel flutter under supersonic flow with random fluctuations in the turbulent boundary layer. Nonstandard reduction through stochastic averaging has been done to reduce the system. They have shown that qualitatively different density functions for the response are obtained as some of the system parameters are varied. Lindsley et al. [47] have also studied limit cycle oscillation of nonlinear square panels under supersonic flow with uncertainties in the modulus of elasticity and boundary conditions. Effect of these uncertainties on the panel limit cycle oscillation has been observed using Monte Carlo simulations. Shubov [48,49] has presented a comprehensive review of various research directions of aeroelastic flutter. Several mathematical models have been discussed with and without external loading in both probabilistic and deterministic frameworks.

The focus of this paper is to demonstrate the use of arbitrary polynomial chaos in capturing the propagation of uncertainty through the aeroelastic stall flutter system. In the next section, a discussion on the arbitrary polynomial chaos is introduced. In Section 3, the equation of motion for the single-degree-of-freedom stall oscillation system being studied in this paper, is presented in the nondimensional form. The aerodynamic loading on the structure, computed using the Onera dynamic stall model, is presented in Section 4. In Section 5, the polynomial chaos expansion formulation for the stall flutter system for two different input uncertainties is derived. Numerical results are presented in Section 6. Finally in Section 7, to conclude, some comments are made based on the study carried out in this paper.

2. Arbitrary polynomial chaos expansion

In the present paper parametric uncertainties in the stall flutter problem are modeled using arbitrary polynomial chaos (APC). Arbitrary polynomial chaos is a combination of the polynomial chaos expansion and an orthogonalization

method. Orthogonalization is employed to construct an appropriate set of expansion polynomials for arbitrary input distributions. Gram–Schmidt orthogonalization is used to construct the polynomials based on the statistical moments of the uncertain input.

2.1. Polynomial chaos

The stall flutter problem is modeled by a differential equation of motion and the system of differential equations of the Onera dynamic stall model. Modeling uncertainties in the stall flutter problem results in a system of stochastic differential equations, which are based on a probability space $(\mathbf{\Omega}, \sigma, P)$. Let $\omega \in [0,1]$ be an element of the sample space $\mathbf{\Omega}$. Then an uncertain variable $u(t,\omega)$ is denoted by the argument ω to emphasize the fact that an uncertain variable is a function of a random event. Suppose that the stall flutter model is described by the following differential equation for $u(t,\omega)$ with operator $\mathscr{L}$ and source term S

$$\mathscr{L}(t,\omega;u(t,\omega)) = S(t,\omega), \tag{1}$$

with time t and appropriate initial conditions. The uncertainty is given by uncertain input parameters with known probability distribution. The uncertain variable $u(t,\omega)$ and the uncertain parameters can be represented by a polynomial chaos expansion

$$u(t,\omega) = \sum_{i=0}^{\infty} u_i(t)\mathbf{\Psi}_i(\boldsymbol{\xi}(\omega)), \tag{2}$$

where $\{u_i(t)\}$ denote the deterministic polynomial chaos coefficients and $\{\mathbf{\Psi}_i(\boldsymbol{\xi}(\omega))\}$ denote multidimensional orthogonal polynomials in terms of an n-dimensional vector of random variables $\boldsymbol{\xi}(\omega) = (\xi_1(\omega), \ldots, \xi_n(\omega))$, where n is the number of uncertain parameters. The polynomials $\{\mathbf{\Psi}_i(\boldsymbol{\xi}(\omega))\}$ satisfy the following orthogonality relation:

$$\langle \mathbf{\Psi}_i(\boldsymbol{\xi}), \mathbf{\Psi}_j(\boldsymbol{\xi})\rangle = \langle \mathbf{\Psi}_i^2(\boldsymbol{\xi})\rangle \delta_{ij}, \tag{3}$$

where δ_{ij} denotes the Kronecker delta and $\langle\cdot,\cdot\rangle$ denotes the inner product over the space of functions mapping $\mathbf{\Omega}$ onto the real line $\mathbb{R}$

$$\begin{aligned}\langle \mathbf{\Psi}_i(\boldsymbol{\xi}), \mathbf{\Psi}_j(\boldsymbol{\xi})\rangle &= \int_{\mathbf{\Omega}} \mathbf{\Psi}_i(\boldsymbol{\xi})\mathbf{\Psi}_j(\boldsymbol{\xi})\,\mathrm{d}P \\ &= \int_{\mathrm{supp}_{\boldsymbol{\xi}}} \mathbf{\Psi}_i(\boldsymbol{\xi})\mathbf{\Psi}_j(\boldsymbol{\xi}) p_{\boldsymbol{\xi}}(\boldsymbol{\xi})\,\mathrm{d}\boldsymbol{\xi},\end{aligned} \tag{4}$$

where $\mathrm{d}P$ is the probability measure of the random variables $\boldsymbol{\xi}(\omega)$, $p_{\boldsymbol{\xi}}(\boldsymbol{\xi})$ is the corresponding weighting function and the probability density of $\boldsymbol{\xi}(\omega)$, and $\mathrm{supp}_{\boldsymbol{\xi}}$ is the support of $\boldsymbol{\xi}$. The deterministic coefficients can be solved for numerically using a stochastic finite element approach [21]. For the numerical implementation the infinite summation in (2) is truncated at the $(N+1)$th term, with

$$(N+1) = \frac{(n+p)!}{n!p!}, \tag{5}$$

where p is the highest order of the polynomials $\{\mathbf{\Psi}_i(\boldsymbol{\xi})\}_{i=0}^{N}$. Substituting the truncated polynomial chaos expansions (2) of the uncertain variables and the uncertain parameters into the governing Equation (1) results in

$$\mathscr{L}\left(t,\omega;\sum_{i=0}^{N} u_i(t)\mathbf{\Psi}_i(\boldsymbol{\xi})\right) \approx S(t,\omega). \tag{6}$$

A stochastic Galerkin approach is employed to obtain a system of $(N+1)$ deterministic equations for the $(N+1)$ deterministic coefficients. The Galerkin projection of (6) in the probability space onto each polynomial basis $\{\mathbf{\Psi}_i(\boldsymbol{\xi})\}_{i=0}^{N}$ in the sense of inner product (4) yields

$$\left\langle \mathscr{L}\left(t,\omega;\sum_{i=0}^{N} u_i(t)\mathbf{\Psi}_i(\boldsymbol{\xi})\right), \mathbf{\Psi}_j(\boldsymbol{\xi})\right\rangle = \langle S(t,\omega), \mathbf{\Psi}_j(\boldsymbol{\xi})\rangle, \tag{7}$$

for $j = 0,1,\ldots,N$. This system of deterministic equations can be solved numerically using standard discretization and iteration methods.

In the original homogeneous polynomial chaos [21] the probability measure is the Gaussian measure and the random variables $\boldsymbol{\xi}(\omega)$ are Gaussian random variables. In that case the polynomials $\{\mathbf{\Psi}_i(\boldsymbol{\xi})\}$ which satisfy the orthogonality relation (3) are Hermite polynomials. It is demonstrated that the homogeneous polynomial chaos can achieve exponential convergence for Gaussian input uncertainties [25]. For several other standard distributions, the appropriate polynomials are other orthogonal polynomials of the Askey scheme [26]. For example the Laguerre and Jacobi polynomials are orthogonal with respect to the gamma and beta distribution. In [26] it has been demonstrated that these polynomials can achieve exponential convergence for the corresponding input distributions. Often the input distributions do not correspond to classical orthogonal polynomials. In that case appropriate polynomials $\{\mathbf{\Psi}_i(\boldsymbol{\xi})\}$ orthogonal with respect to an arbitrary probability measure can be constructed using an orthogonalization method [27,32]. The random variables $\{\xi_i(\omega)\}$ are then obtained from linear transformations of the uncertain input parameters to corresponding standard domains, i.e. $[-1,1]$, $[0,\infty)$ or $(-\infty,\infty)$. This approach is referred to as arbitrary polynomial chaos.

2.2. Construction of the orthogonal polynomials

The appropriate polynomials $\{\mathbf{\Psi}_i(\boldsymbol{\xi})\}$ for a polynomial chaos expansion are orthogonal with respect to the probability density of the uncertain input, $p_{\boldsymbol{\xi}}(\boldsymbol{\xi})$ in (4). In the arbitrary polynomial chaos, Gram–Schmidt orthogonalization is employed to construct the polynomials based on statistical moments of the uncertain input [32].

The problem of finding a set of polynomials $\{\mathbf{\Psi}_i(\boldsymbol{\xi})\}_{i=0}^{N}$ orthogonal with respect to a given weighting function is an orthogonal basis problem given by Eqs. (3) and (4). Gram–Schmidt orthogonalization [50,51] is used to construct the one-dimensional orthogonal polynomials $\{\Psi_i(\xi)\}_{i=0}^{p}$. The multidimensional orthogonal polynomials

$\{\boldsymbol{\Psi}_i(\boldsymbol{\xi})\}_{i=0}^{N}$ are given by the tensor product of the one-dimensional polynomials $\{\Psi_i(\xi)\}_{i=0}^{p}$. A set of one-dimensional ($n=1$) monic orthogonal polynomials, i.e. $\{\Psi_i(\xi)\}_{i=0}^{p}$ with $\Psi_i(\xi)=\xi^i+\mathcal{O}(\xi^{i-1})$, $i=0,1,\ldots,p$, can be computed using the classical Gram–Schmidt algorithm by recursively generating

$$\Psi_i(\xi)=e_i(\xi)-\sum_{j=0}^{i-1}c_{ij}\Psi_j(\xi),\quad i=1,2,\ldots,p, \tag{8}$$

with $\Psi_0=1$ and

$$c_{ij}=\frac{\langle e_i(\xi),\Psi_j(\xi)\rangle}{\langle \Psi_j(\xi),\Psi_j(\xi)\rangle}, \tag{9}$$

where the polynomials $\{e_i(\xi)\}$ are polynomials of exact degree i. The inner products in Eq. (9) are determined by using the statistical moments of the uncertain input. The orthogonal polynomials $\{\Psi_i(\xi)\}_{i=0}^{p}$ are written as a summation of monomial terms

$$\Psi_i=\sum_{I=0}^{i}c_{i,I}\xi^I. \tag{10}$$

The inner products of the polynomials in Eq. (9) can then be written as a summation over the statistical moments of the uncertain input

$$\begin{aligned}\langle \Psi_i(\xi),\Psi_j(\xi)\rangle &= \int_{\mathrm{supp}_\xi}\Psi_i(\xi)\Psi_j(\xi)p_\xi(\xi)\,\mathrm{d}\xi\\ &=\sum_{I=0}^{i}\sum_{J=0}^{j}c_{i,I}c_{j,J}\mu_{\xi,I+J}\end{aligned} \tag{11}$$

with $\mu_{\xi,i}$ the ith raw moment of $\xi(\omega)$

$$\mu_{\xi,i}=\int_{\mathrm{supp}_\xi}\xi^i p_\xi(\xi)\,\mathrm{d}\xi. \tag{12}$$

For many important uncertainty distribution the raw moments are known in analytical form. For example for the lognormal distribution they are given by

$$\mu_{\xi,i}=\mathrm{e}^{iM_{\ln}+\frac{1}{2}(iS_{\ln})^2} \tag{13}$$

with $M_{\ln}$ and $S_{\ln}$ two parameters of the lognormal probability density function

$$p_{\mathrm{lognormal}}(\xi)=\frac{1}{\xi S_{\ln}\sqrt{2\pi}}\mathrm{e}^{-(\ln\xi-M_{\ln})^2/2S^2}. \tag{14}$$

Virtually no computational costs are associated with constructing the appropriate orthogonal polynomials in this way. For distributions of which the raw moments are not known analytically, the moments can be computed numerically in an efficient way using Gauss quadrature integration. This results in a computational work of $\mathcal{O}(N_{\mathrm{ip}}N)$, where $\mathrm{N_{ip}}$ is the number of discrete points for the inner products and $(N+1)$ is the number of terms of the polynomial chaos expansion. The modified Gram–Schmidt algorithm with one reorthogonalization step is implemented.

3. Equation of motion

To derive the equation of motion of a two-dimensional blade section, we consider a strip of unit span of a symmetric airfoil. Here, a NACA 0012 profile is considered. A schematic plot of the structure and its coordinate system is given in Fig. 1. The pitching oscillation represents the classical stall flutter case of an airfoil predominantly vibrating in the torsional direction. The equation of motion for the single degree-of-freedom pitching oscillation is given below [4,10]:

$$I_\alpha\ddot{\alpha}+I_\alpha\omega_\alpha^2\alpha+K_{\mathrm{nl1}}\alpha^3=M(t). \tag{15}$$

Here, I_α is the wing mass moment of inertia; α is the effective angle of attack; ω_α is the natural frequency of the pitch elastic mode; K_{nl1} is a nonlinear stiffness term accounting for concentrated structural nonlinearities in the torsional direction; $M(t)$ is the time dependent aerodynamic moment. A nondimensional form of the governing equation is often helpful in aeroelastic analysis to investigate the effect of system parameters. A nondimensional form of the above Eq. (15) [4,10] is

$$\alpha''+\alpha/(U^2)+K_{\mathrm{nl}}\alpha^3=2C_{\mathrm{m}}/(\pi\mu r_\alpha^2). \tag{16}$$

Here, $(')$ is denoted as derivative with respect to nondimensional time $\tau=t\overline{V}/b$; $\overline{V}$ is the resultant wind speed as shown is Fig. 1; b is the semi-chord of the blade; C_{m} is the moment coefficient which is given by the Onera dynamic stall model discussed in the next section; U is the nondimensional airspeed defined as $U=\overline{V}/b\omega_\alpha$; μ and r_α are nondimensional structural parameters; mass ratio $\mu=m/(\pi\rho b^2)$; radius of gyration $r_\alpha=I_\alpha/(mb^2)$; K_{nl} is the nondimensional form of K_{nl1}.

In the original dimensional model of Eq. (15), a concentrated structural nonlinearity is incorporated in the form of a cubic stiffness $K_{\mathrm{nl1}}\alpha^3$. As has already been discussed, this artifice has been used in the literature to model the

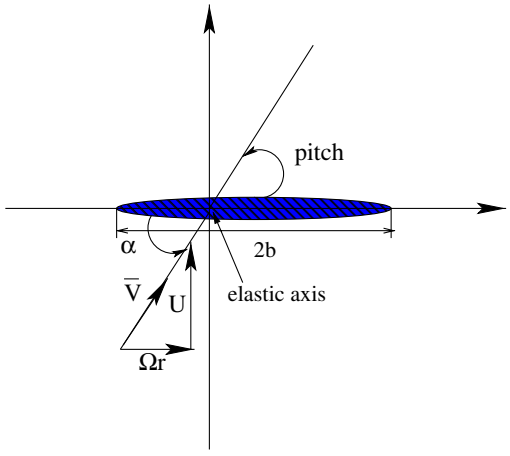

Fig. 1. Schematic plot of the airfoil coordinate system and oscillation degree-of-freedom.

stiffening spring behavior of a blade being twisted [8]. Also, this is often a standard way to consider some control mechanisms that may be present in the structure [5,7].

4. Onera dynamic stall model

The Onera stall model gives the aerodynamic loads in the form of differential equations. This is a semi-empirical method, which relies on experimental data to fit the coefficients of the differential equations. The physical process of dynamic stall involves leading and trailing edge vortex development and their subsequent separation and shedding into the wake. Vortex growth increases suction and helps increase the aerodynamic loads beyond their static stall values. Vortex separation from the body triggers a rapid decrease of the loads. The Onera model takes into account this complex unsteady phenomena step by step. The aerodynamic loads by the Onera model are given in two parts; the inviscid part, and the viscous part which becomes important above the static stall angle.

For a detailed discussion of the Onera dynamic stall model see [16,17]. We give the equations for aerodynamic load coefficients by Onera below [4]:

$$C_z = s_z\alpha' + k_{vz}\theta'' + C_{z1} + C_{z2},$$

$$C'_{z1} + \lambda_z C_{z1} = \lambda_z(a_{oz}\alpha + \sigma_z\theta') + \alpha_z(a_{oz}\alpha' + \sigma_z\theta''), \tag{17}$$

$$C''_{z2} + 2dwC'_{z2} + w^2(1+d^2)C_{z2} = -w^2(1+d^2)(\Delta C_z|\alpha + e\Delta C'_z|\alpha). \tag{18}$$

Here, θ is the pitching angle and α is the total angle of attack $\theta - \dot{h}$, h is the flapping displacement; C_z refers to any aerodynamic load coefficients C_L, C_D, or C_M; C_{z1} is the inviscid circulatory part of the load and C_{z2} is the viscous part; $s_z, k_{vz}, \lambda_z, \alpha_z, a_{oz}, \sigma_z, d, w$ and e are the coefficients associated with the aerodynamic forces; these coefficients are determined empirically by parameter identification techniques using experimental data. The coefficients used in this study have been taken from Dunn and Dugundji [17] for a NACA 0012 profile.

The differential equation for each part has been modeled in such a way that the mathematical model resembles the complex physical process of dynamic stall as closely as possible. The first-order inviscid equation (17) expresses a single lag term operating on the linear part of an airfoil's static force. It represents the increase of aerodynamic loads beyond the static stall angle. The coefficients of this part are obtained from steady state experiments and are dependent on the airfoil profile. The viscous part, Eq. (18), takes care of the decrease of the loads during the dynamic stall hysteresis loop. This equation needs unsteady experimental results; the coefficients, therefore, are dependent on dynamic parameters like frequency. ΔC_z part of the viscous equation refers to the difference in the aerodynamic loads between inviscid and actual(viscous) load at any α greater than the static stall angle. Below the static stall angle ΔC_z is zero. The functions ΔC_z and $\Delta C'_z$ are complex nonlinear functions of α including a step function.

5. Polynomial chaos formulation of the stall flutter system

As mentioned before, uncertainty quantification for aeroelastic problems is a relatively recent trend in the literature. With problems related to flutter, most studies have focused on panel flutter. To the best of our knowledge, no attempt has been made so far to address a stall flutter problem in the uncertainty framework. In this paper, we study the effect on stall flutter due to two uncertain input parameters which have a strong influence on the system response: structural natural frequency and the structural nonlinearity.

The propagation of the uncertainties through the stall flutter system are captured by using arbitrary polynomial chaos. The appropriate expansion polynomials are constructed using Gram–Schmidt orthogonalization based on the statistical moments of the uncertain input. In this section the arbitrary polynomial chaos formulation of the stall flutter problem equation (16) is derived for the two uncertain parameters. This results in a system of deterministic differential equations, which is solved in the time domain for each random mode. In the next section numerical results are presented based on the formulations derived in this section.

5.1. Uncertain structural natural frequency

A deterministic study has demonstrated that the system response is sensitive to variations in the rotational natural frequency of the structure ω_α. Therefore, the uncertainty in $\omega_\alpha(\omega)$ is taken into account and it is assumed to be lognormally distributed with mean μ_{ω_α} and variance $\sigma^2_{\omega_\alpha}$. In the nondimensional formulation of the equation of motion equation (16), the natural frequency $\omega_\alpha(\omega)$ appears in the relation for the nondimensional wind speed $U(\omega) = \overline{V}/b\omega_\alpha(\omega)$. For the polynomial chaos formulation, the variable $\kappa(\omega) = 1/U(\omega)^2$ is introduced. For this case the nonlinear spring stiffness is assumed to be zero. The polynomial chaos expansion for the system response, i.e., the angle of attack $\alpha(\tau,\omega)$, is

$$\alpha(\tau,\omega) = \sum_{i=0}^{p} \alpha_i(\tau)\Psi_i(\xi(\omega)). \tag{19}$$

As uncertain input variable $\kappa(\omega)$ is considered with polynomial chaos expansion

$$\kappa(\omega) = \sum_{j=0}^{1} \kappa_j \Psi_j(\xi(\omega)), \tag{20}$$

where $\xi(\omega)$ is a linear transformation of $\kappa(\omega)$. Substituting these expressions into Eq. (16) results in

$$\sum_{i=0}^{p}\alpha_i''\Psi_i+\sum_{j=0}^{1}\kappa_j\Psi_j\sum_{i=0}^{p}\alpha_i\Psi_i = \frac{2}{\pi\mu r_\alpha^2}\left(s_{\mathrm{m}}\sum_{i=0}^{p}\alpha_i'\Psi_i+k_{\mathrm{vm}}\sum_{i=0}^{p}\alpha_i''\Psi_i + \sum_{i=0}^{p}C_{\mathrm{m1}_i}\Psi_i+\sum_{i=0}^{p}C_{\mathrm{m2}_i}\Psi_i\right). \tag{21}$$

The relations for C_{m1} and C_{m2} given by Eqs. (17) and (18) are also written in a polynomial chaos formulation. The coefficients of Eq. (17), s_{m}, k_{vm}, λ_{m}, α_{m}, a_{om} and σ_{m} are constants. However, the coefficients of the viscous equation (18) $d(\alpha)$, $w(\alpha)$, $e(\alpha)$, $\Delta C_{\mathrm{m}}(\alpha)$ and $\Delta C'_{\mathrm{m}}(\alpha)$ are functions of instantaneous aerodynamic force coefficients, that is, they are functions of $\alpha(\tau,\omega)$. The polynomial chaos formulation of the equation for C_{m1} Eq. (17) is

$$\sum_{j=0}^{p}C'_{\mathrm{m1}_j}\Psi_j+\lambda_{\mathrm{m}}\sum_{j=0}^{p}C_{\mathrm{m1}_j}\Psi_j = \lambda_{\mathrm{m}}\left(a_{\mathrm{om}}\sum_{i=0}^{p}\alpha_i\Psi_i+\sigma_{\mathrm{m}}\sum_{i=0}^{p}\alpha_i'\Psi_i\right) + \alpha_{\mathrm{m}}\left(a_{\mathrm{om}}\sum_{i=0}^{p}\alpha_i'\Psi_i+\sigma_{\mathrm{m}}\sum_{i=0}^{p}\alpha_i''\Psi_i\right). \tag{22}$$

Similarly, for the equation for C_{m2} Eq. (18)

$$\begin{aligned}&\sum_{j=0}^{p}C''_{\mathrm{m2}_j}\Psi_j+2d\left(\sum_{i=0}^{p}\alpha_i\Psi_i\right)w\left(\sum_{i=0}^{p}\alpha_i\Psi_i\right)\sum_{j=0}^{p}C'_{\mathrm{m2}_j}\Psi_j\\ &+w\left(\sum_{i=0}^{p}\alpha_i\Psi_i\right)^2\left(1+d\left(\sum_{i=0}^{p}\alpha_i\Psi_i\right)^2\right)\sum_{j=0}^{p}C_{\mathrm{m2}_j}\Psi_j\\ &=-w\left(\sum_{i=0}^{p}\alpha_i\Psi_i\right)^2\left(1+d\left(\sum_{i=0}^{p}\alpha_i\Psi_i\right)^2\right)\Delta C_{\mathrm{m}}\left(\sum_{i=0}^{p}\alpha_i\Psi_i\right)\\ &\quad-w\left(\sum_{i=0}^{p}\alpha_i\Psi_i\right)^2\left(1+d\left(\sum_{i=0}^{p}\alpha_i\Psi_i\right)^2\right)e\left(\sum_{i=0}^{p}\alpha_i\Psi_i\right)\Delta C'_{\mathrm{m}}\left(\sum_{i=0}^{p}\alpha_i\Psi_i\right).\end{aligned} \tag{23}$$

A Galerkin projection of these equations onto each polynomial basis $\{\Psi_k\}$ is performed in order to minimize the error in each orthogonal direction spanned by the basis functions. By projecting with $\langle\cdot,\Psi_k\rangle$ for $k=\{0,1,\ldots,p\}$ and using the orthogonality relation of the polynomial basis, we obtain the following equations from Eqs. (21) and (22):

$$\alpha_k''+\sum_{i=0}^{p}\hat{\kappa}_{ik}\alpha_i=\frac{2}{\pi\mu r_\alpha^2}(s_{\mathrm{m}}\alpha_k'+k_{\mathrm{vm}}\alpha_k''+C_{\mathrm{m1}_k}+C_{\mathrm{m2}_k}) \tag{24}$$

$$C'_{\mathrm{m1}_k}+\lambda_{\mathrm{m}}C_{\mathrm{m1}_k}=\lambda_{\mathrm{m}}(a_{\mathrm{om}}\alpha_k+\sigma_{\mathrm{m}}\alpha_k')+\alpha_{\mathrm{m}}(a_{\mathrm{om}}\alpha_k'+\sigma_{\mathrm{m}}\alpha_k''), \tag{25}$$

and, similarly, from Eq. (23):

$$\begin{aligned}&C''_{\mathrm{m2}_k}+\sum_{j=0}^{p}2\left\langle d\left(\sum_{i=0}^{p}\alpha_i\Psi_i\right)w\left(\sum_{i=0}^{p}\alpha_i\Psi_i\right)\Psi_j,\Psi_k\right\rangle C_{\mathrm{m2}_j}\\ &+\sum_{j=0}^{p}\left\langle w\left(\sum_{i=0}^{p}\alpha_i\Psi_i\right)\left(1+d\left(\sum_{i=0}^{p}\alpha_i\Psi_i\right)^2\right)\Psi_j,\Psi_k\right\rangle C_{\mathrm{m2}_j}\\ &=-\left\langle w\left(\sum_{i=0}^{p}\alpha_i\Psi_i\right)^2\left(1+d\left(\sum_{i=0}^{p}\alpha_i\Psi_i\right)^2\right)\Delta C_{\mathrm{m}}\left(\sum_{i=0}^{p}\alpha_i\Psi_i\right),\Psi_k\right\rangle\\ &\quad-\left\langle w\left(\sum_{i=0}^{p}\alpha_i\Psi_i\right)^2\left(1+d\left(\sum_{i=0}^{p}\alpha_i\Psi_i\right)^2\right)e\left(\sum_{i=0}^{p}\alpha_i\Psi_i\right)\Delta C'_{\mathrm{m}}\left(\sum_{i=0}^{p}\alpha_i\Psi_i\right),\Psi_k\right\rangle,\end{aligned} \tag{26}$$

for $k=0,1,\ldots,p$, where $\hat{\kappa}_{ik}$ in Eq. (24) is given by

$$\hat{\kappa}_{ik}=\frac{1}{\langle\Psi_k^2\rangle}\sum_{j=0}^{1}\langle\Psi_i\Psi_j\Psi_k\rangle\kappa_j, \tag{27}$$

for $i,k=0,1,\ldots,p$. For each k, the above set of differential equations are solved in the time domain using a fourth-order Runge–Kutta time integration scheme.

5.2. Uncertain structural nonlinearity

A second parameter to which the flutter system is sensitive is the geometric nonlinear structure parameter K_{nl}. Next the nonlinear stiffness $K_{\mathrm{nl}}(\omega)$ is considered as an uncertain parameter with a lognormal distribution with mean $\mu_{K_{\mathrm{nl}}}$ and variance $\sigma^2_{K_{\mathrm{nl}}}$. The polynomial chaos formulation of the flutter system equations (16)–(18) subject to an uncertain K_{nl} is similar to the equations derived in the previous section. The system response $\alpha(\omega)$ is expanded in the polynomial chaos expansion of Eq. (19). Substituting $\alpha(\omega)$ and $K_{\mathrm{nl}}(\omega)$ in the chaos expansion form in Eq. (16), the third term at the left hand side of Eq. (16) becomes

$$K_{\mathrm{nl}}\alpha^3=\sum_{j=0}^{1}K_{\mathrm{nl}_i}\Psi_j\sum_{i_1=0}^{p}\sum_{i_2=0}^{p}\sum_{i_3=0}^{p}\alpha_{i_1}\alpha_{i_2}\alpha_{i_3}\Psi_{i_1}\Psi_{i_2}\Psi_{i_3}. \tag{28}$$

Using a Galerkin projection $\langle\cdot,\Psi_k\rangle$, the above term becomes

$$\left\langle\sum_{j=0}^{1}K_{\mathrm{nl}_j}\Psi_j\sum_{i_1=0}^{p}\sum_{i_2=0}^{p}\sum_{i_3=0}^{p}\alpha_{i_1}\alpha_{i_2}\alpha_{i_3}\Psi_{i_1}\Psi_{i_2}\Psi_{i_3},\Psi_k\right\rangle = \sum_{i_1=0}^{p}\sum_{i_2=0}^{p}\sum_{i_3=0}^{p}\hat{K}_{\mathrm{nl}_{i_1i_2i_3k}}\alpha_{i_1}\alpha_{i_2}\alpha_{i_3}, \tag{29}$$

where $\hat{K}_{\mathrm{nl}_{i_1i_2i_3k}}$ is defined as

$$\hat{K}_{\mathrm{nl}_{i_1i_2i_3k}}=\frac{1}{\langle\Psi_k^2\rangle}\sum_{j=0}^{1}\langle\Psi_{i_1}\Psi_{i_2}\Psi_{i_3}\Psi_j\Psi_k\rangle K_{\mathrm{nl}_i} \tag{30}$$

with $i_1,i_2,i_3,\ k=0,1,\ldots,p$. The right hand side of Eq. (21) after chaos expansion and Galerkin projection is evaluated in the same manner as shown in the previous case.

6. Results

In this section numerical results are presented for the polynomial chaos formulations derived in the previous

section. The two non-negative input parameters describing the structural natural frequency and the structural nonlinearity are assumed to be uncertain with an lognormal distribution. The appropriate basis polynomials for the lognormal input distributions are constructed within the arbitrary polynomial chaos framework by Gram–Schmidt orthogonalization as described in Section 2.2.

6.1. Uncertain structural natural frequency

In this case the torsional natural frequency ω_α is assumed to be lognormally distributed and the structural nonlinearity term K_{nl} is assumed to be zero. To evaluate the inner products involving the complex nonlinear functions ΔC_{m} and $\Delta C'_{\mathrm{m}}$ in Eq. (26) a numerical integration scheme using Simpson's rule is employed. After the chaos expansion and the Galerkin projection, aeroelastic differential equations in each of the $p+1$ random modes are solved in the time domain using a fourth-order Runge–Kutta direct integration method with a nondimensional time step of $\Delta\tau = 0.01$. This time step size satisfies the convergence criterion and also is small enough with respect to the frequency of oscillations.

The natural frequency ω_α appears in the nondimensional formulation in the relation for the nondimensional wind speed U. In Fig. 2 the deterministic bifurcation diagram is presented with U being the bifurcation parameter. The bifurcation diagram shows the subcritical Hopf bifurcation around $U = 16$ (U_{cr}). For all the different cases of U shown in this figure, time histories are generated using an initial angular perturbation of 10° about a mean angle of attack of 4°. At the critical value of U, the airfoil enters the dynamic stall regime, past the stall angle of 12° and a limit cycle oscillation starts [19]. It is important to note that the limit cycle oscillation starts as soon as the response crosses past the linear aerodynamic region, that is, past the static stall angle. To present a realistic example, for a typical 1000 kW wind turbine, at a 0.75 blade radius test section with semi-chord $b = 0.8$ m and resultant wind speed $\overline{V} = 50$ m/s, the deterministic result points that the critical value of ω_α would be 3.9 rad/s [52,53].

Subsequently, in the uncertainty analysis, we take two different mean values for ω_α: $\mu_{\omega_\alpha} = 6.25$ rad/s in the linear aerodynamic regime and $\mu_{\omega_\alpha} = 3.68$ rad/s, in the nonlinear, dynamic stall region. In both cases, the coefficient of variation is 1.5%. The focus is to examine the performance of polynomial chaos expansions in capturing the uncertainty in the aeroelastic response in both the linear and nonlinear regimes. The polynomial chaos expansion results are compared with standard Monte Carlo simulations with 1000 realizations.

For $\mu_{\omega_\alpha} = 6.25$ rad/s the distribution of the nondimensional natural frequency $\overline{\omega}_\alpha$ is shown in Fig. 3, with $\overline{\omega}_\alpha = \omega_\alpha(\omega) b/\overline{V}$. The corresponding value of U is for this case equal to 10. The deterministic study points out that in this range of U, the response is a damped oscillation, or, in other words, converges to a stable fixed point. The distribution of the damped response α computed using the APC technique is presented in Fig. 4 with respect to the random event ω. Monte Carlo simulation (MC) results are also presented in the same plot. We observe, the match is almost exact at every range of the ω spectrum. A typical time history at $\omega = 0.9$ ($U = 10.196$), generated using the APC results is presented in Fig. 5 and compared with the corresponding realization from the MC results. The response time history as predicted by APC calculations matches exactly with that of the MC analysis. A fourth-order expansion has been used for the APC model and is seen to be enough to capture the response well in this linear range of the problem.

For $\mu_{\omega_\alpha} = 3.68$ rad/s the distribution of $\overline{\omega}_\alpha = \omega_\alpha(\omega) b/\overline{V}$ are shown in Fig. 6. This corresponds to a mean value for the dimensional wind speed of $U = 17$. As the deterministic results point out, this falls in the nonlinear aerodynamic regime of dynamic stall and limit cycle oscillations (LCO)

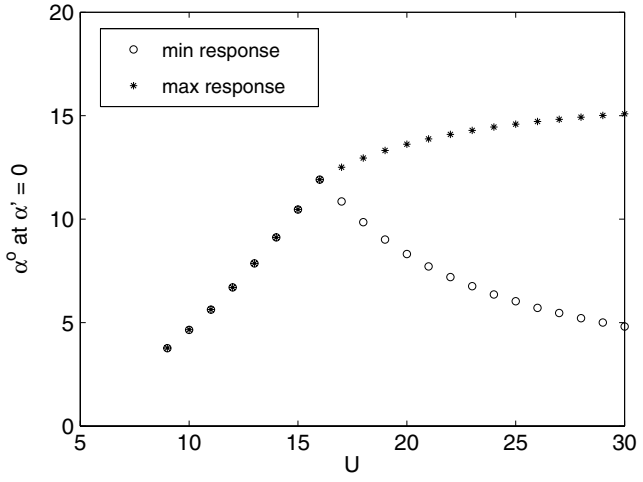

Fig. 2. Bifurcation diagram for the deterministic aeroelastic system.

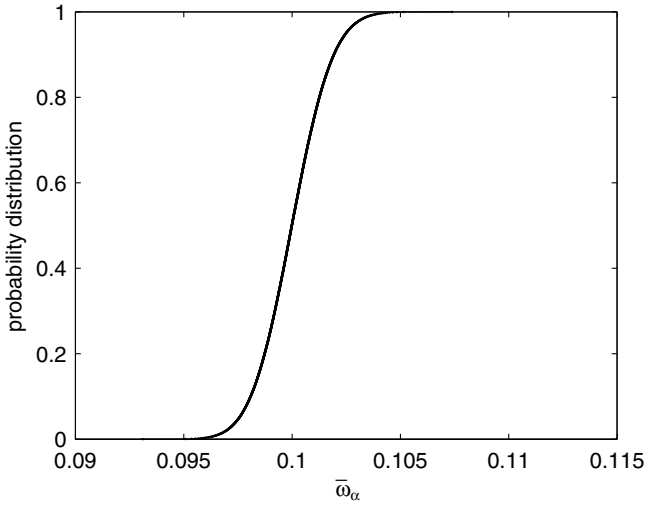

Fig. 3. Lognormal distribution of $\mu_{\overline{\omega}_\alpha} = 1/10$, $\mathrm{COV}_{\overline{\omega}_\alpha} = 1.5\%$.

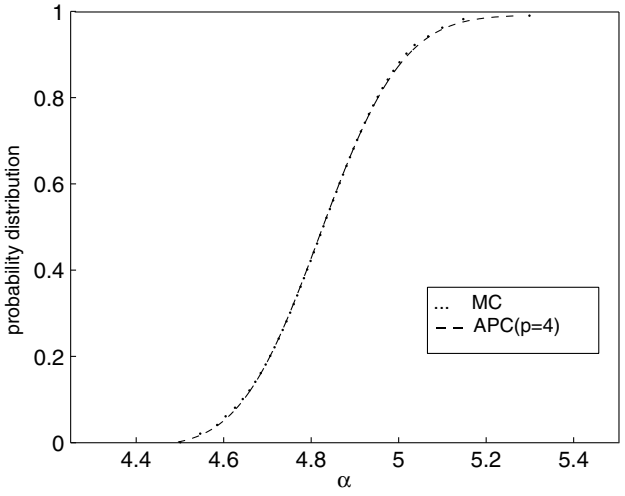

Fig. 4. Probability distribution of response α° by APC and MC for $\mu_{\overline{\omega}_\alpha} = 1/10,\ \mathrm{COV}_{\overline{\omega}_\alpha} = 1.5\%$.

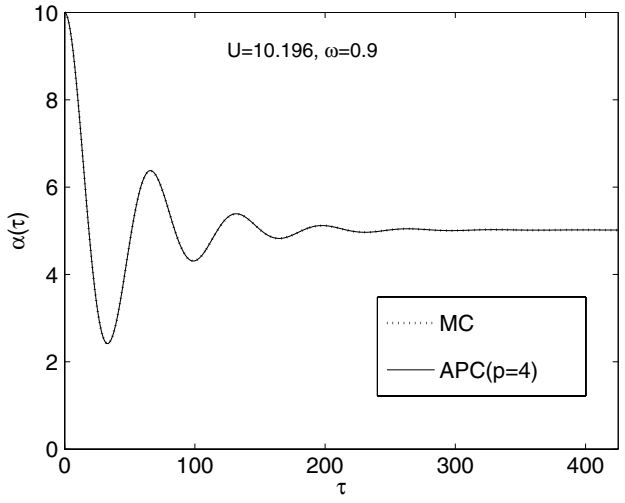

Fig. 5. Comparison of a typical time history by APC and the corresponding MC realization for $\mu_{\overline{\omega}_\alpha} = 1/10,\ \mathrm{COV}_{\overline{\omega}_\alpha} = 1.5\%$.

take place. This case is studied in more detail, because it is more difficult to achieve convergence with polynomial chaos expansions for a nonlinear problem than a linear one [39]. In this case, we present the LCO results in terms of the maximum and minimum amplitudes during one period of oscillation. The probability distributions of the maximum and minimum amplitude are presented in Figs. 7 and 8. The maximum and the minimum branches have been generated using an increasing order (p) of chaos expansion. APC results are compared with standard Monte Carlo simulations with 1000 realizations. It is evident from these figures that the $p = 2$ case clearly does not have enough chaos expansion terms to represent the output. As p increases, the results seem to become better, and with $p = 8$, the APC minimum and maximum values almost exactly match with the MC simulation results. The maximum and minimum amplitude as function of $\overline{\omega}_\alpha$ is given in Fig. 9. It is interest-

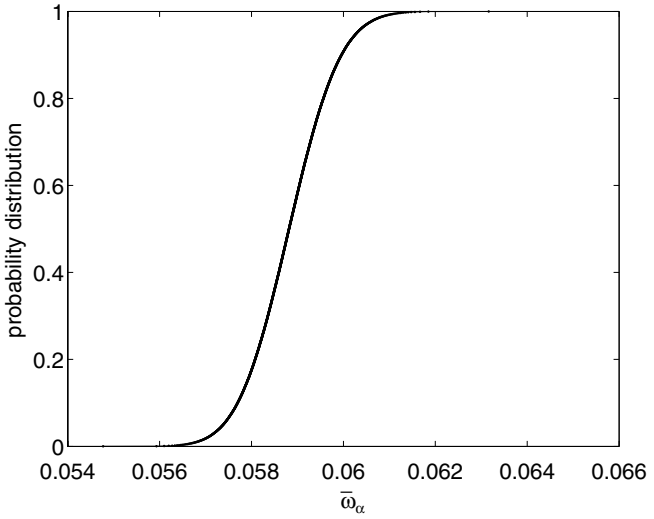

Fig. 6. Lognormal distribution $\mu_{\overline{\omega}_\alpha} = 1/17,\ \mathrm{COV}_{\overline{\omega}_\alpha} = 1.5\%$.

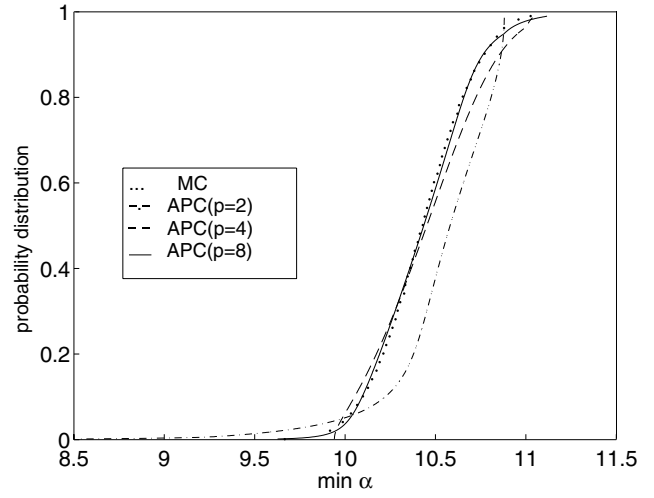

Fig. 7. Probability distribution of minimum value of the response α° by APC and MC for $\mu_{\overline{\omega}_\alpha} = 1/17,\ \mathrm{COV}_{\overline{\omega}_\alpha} = 1.5\%$.

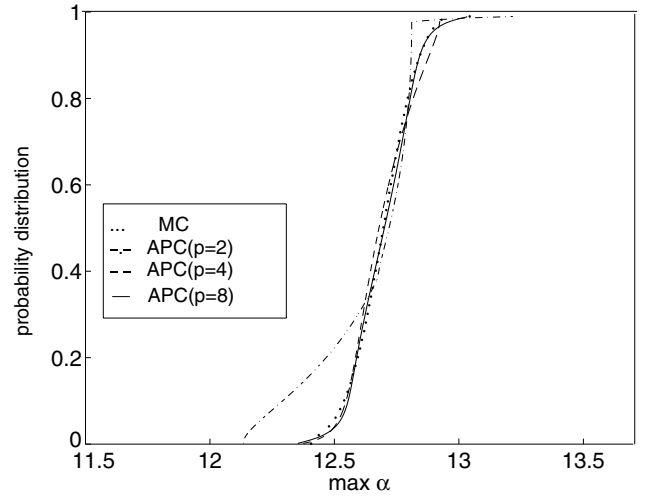

Fig. 8. Probability distribution of maximum value of the response α° by APC and MC for $\mu_{\overline{\omega}_\alpha} = 1/17,\ \mathrm{COV}_{\overline{\omega}_\alpha} = 1.5\%$.

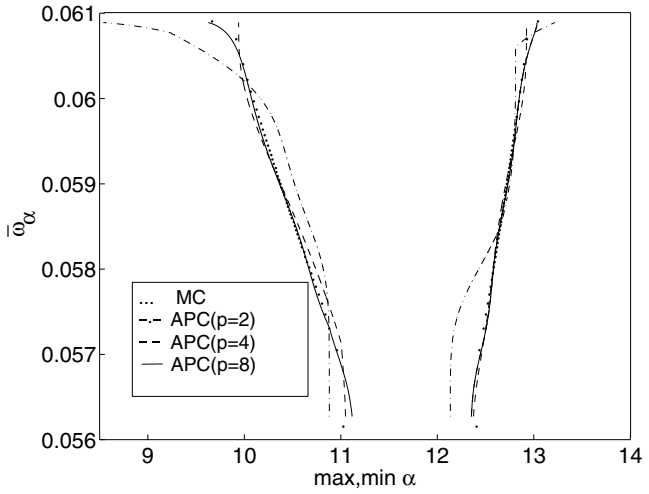

Fig. 9. Variation of the minimum and maximum value of the response α° with $\overline{\omega}_\alpha$ by APC and MC for $\mu_{\overline{\omega}_\alpha} = 1/17,\ \mathrm{COV}_{\overline{\omega}_\alpha} = 1.5\%$.

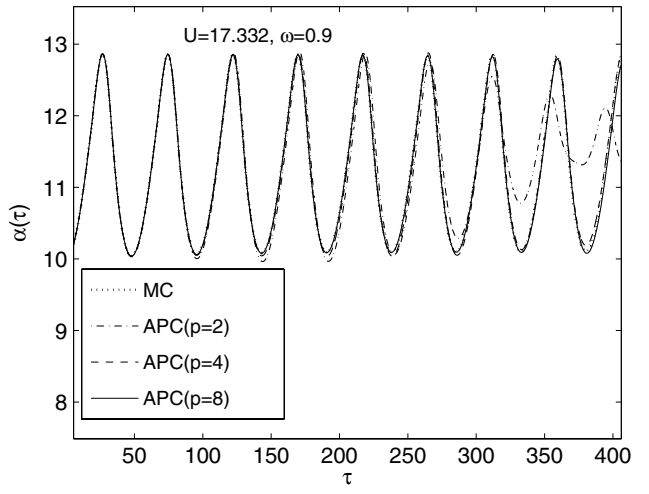

Fig. 10. Comparison of a typical time history by APC and the corresponding MC realization for $\mu_{\overline{\omega}_\alpha} = 1/17,\ \mathrm{COV}_{\overline{\omega}_\alpha} = 1.5\%$.

ing to see a typical time domain results by APC given in Fig. 10. As a representative ω value, the time history results for $\omega = 0.9 (U = 17.332)$ are shown as it is at one tail-end of the ω domain, away from the mean. APC expansion captures the time realization well at small time intervals. However, with longer time we observe the time history degenerate. This was also reported by Pettit and Beran [39,40] when they used Hermite and Legendre polynomials for a limit cycle oscillation. The degeneracy improves as the order of chaos expansion increases, as they have also pointed out. However, even with a large number of expansion terms, this trend could only be delayed but not entirely overcome [39,40]. Hou et al. [54] also face this problem when they used Wiener chaos expansions for stochastic Navier–Stokes equations.

In our APC results, we witness a gradual improvement of the time history with higher p. For example, with $p = 8$, the match with the deterministic result is almost exact within the time window shown till $\tau = 400$, though a gradual degeneracy is observed at much higher times (not shown here). Following this argument, in order to see the variation of the minimum and maximum values of the limit cycle oscillation as was shown in Fig. 9, we use the time cycles within $\tau = 300$. The existence of this degeneracy has been first reported by Millman et al. [42] and has not been discussed in detail till recently [39]. Here the authors argue that for highly nonlinear functions, the nonlinearity of the solution with respect to the random variable increases with time which becomes difficult to model using even a high order of polynomial expansions. It is to be noted that in the linear solution domain, the APC scheme works well as demonstrated by the results in Figs. 4 and 5. Therefore, we conclude that the trend observed here is similar to that observed by previous researchers in capturing LCOs using other PCE schemes. These results show that arbitrary polynomial chaos captures the uncertain stall flutter response in both linear and nonlinear range; and in representing the LCOs in the nonlinear domain it shows the similar trend as shown by other PCE schemes of the Askey chaos family.

6.2. Uncertain structural nonlinearity

In the second part of the study a nonzero structural nonlinearity parameter K_{nl} is considered. This represents a geometric nonlinearity with cubic spring stiffness. The spring stiffness K_{nl} is assumed to be uncertain with a lognormal distribution and ω_α is considered to be deterministic. The mean is $\mu_{K_{\mathrm{nl}}} = 0.05$ and $\sigma^2_{K_{\mathrm{nl}}} = 0.001$. The distribution of K_{nl} is given in Fig. 11. Deterministic results suggest that with $K_{\mathrm{nl}} = 0.05$, the critical U lies in the range of 25–30. Below this value, the response converges to a stable fixed point. We use the APC expansion with $p = 4$ to capture the response in this range of U. For $U = 28$, APC results are presented along with Monte Carlo simulations in

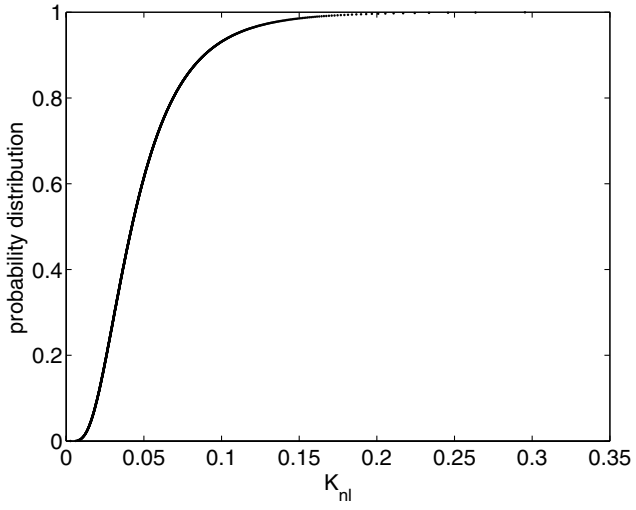

Fig. 11. Lognormal distribution for $\mu_{K_{\mathrm{nl}}} = 0.05, \sigma^2_{K_{\mathrm{nl}}} = 0.001$.

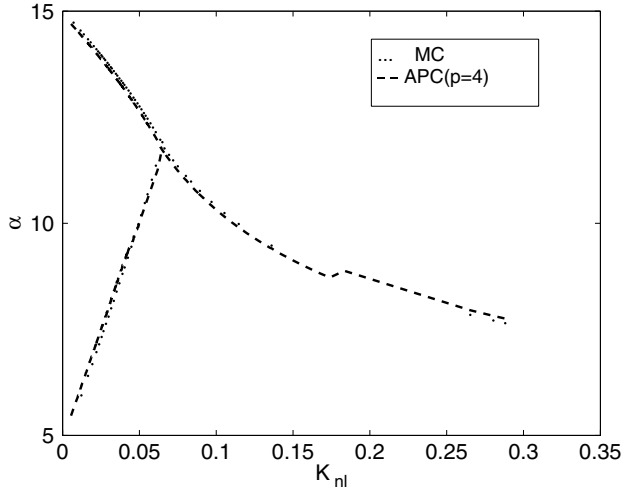

Fig. 12. Minimum and maximum response α° as function of the structural nonlinearity parameter K_{nl} by APC and MC for lognormal distribution $\mu_{K_{\mathrm{nl}}} = 0.05,\ \sigma^2_{K_{\mathrm{nl}}} = 0.001$.

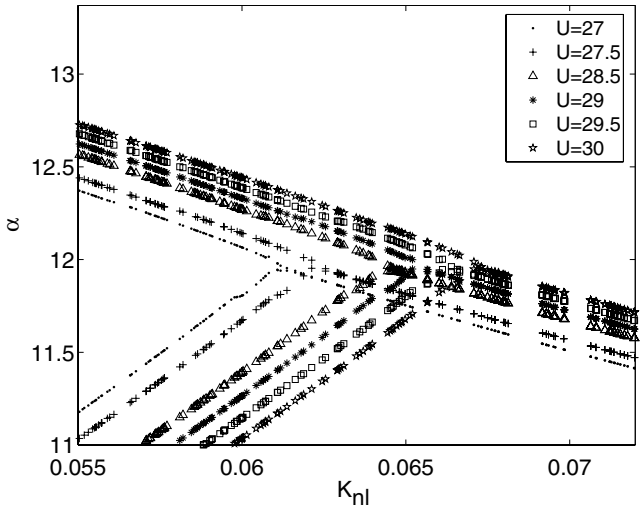

Fig. 14. Onset of limit cycle oscillation as a function of the structural nonlinearity parameter K_{nl}.

Fig. 12. The system response is presented in terms of maximum and minimum angular amplitudes in one cycle of oscillations. At some values of K_{nl}, the maximum and minimum angles of attack overlaps, signifying a damped response. The K_{nl} value at which this occurs is the supercritical Hopf bifurcation point. The comparison of APC and Monte Carlo simulation results are good. We consider APC results at small time range, within which the match of the time histories generated by the APC expansion technique and Monte Carlo realization is reasonable good. We also present the ω versus K_{nl} plot in Fig. 13.

We also present the Monte Carlo results for uncertain K_{nl} variation with different U values between 27 and 30 in Fig. 14. Branches of maximum and minimum values of the response meet at the critical points and indicate the onset of flutter. The critical flutter point of K_{nl} is seen to be increasing along the K_{nl} axis as the U value increases. It should be noted that the critical range of K_{nl} lies in close proximity of the $\mu_{K_{\mathrm{nl}}} = 0.05$ value. It would be worthwhile to consider a much wider range of U in order to identify the critical points pertaining to a broader spectrum of K_{nl} in the bifurcation plane. This may prove to be computationally intensive as the K_{nl} distribution range considered in this work is wide and for that, relevant range of U could be large. To give an example, deterministic results show that for K_{nl}= 0.1, limit cycle oscillations do not appear till U becomes as large as 60.

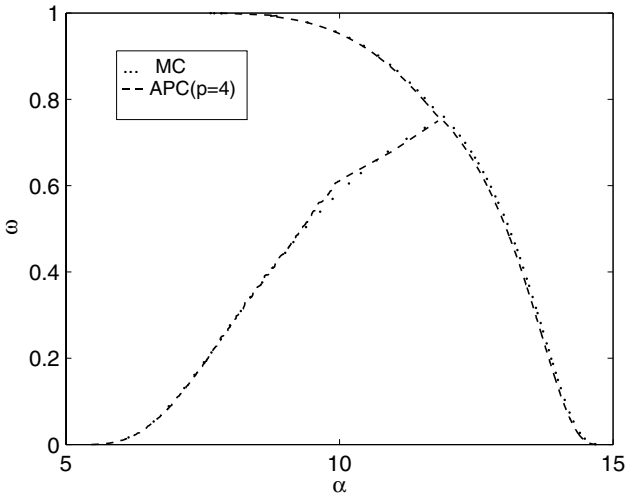

Fig. 13. Minimum and maximum response α° as function of ω by APC and MC for lognormal distribution $\mu_{K_{\mathrm{nl}}} = 0.05,\ \sigma^2_{K_{\mathrm{nl}}} = 0.001$.

At this point, the findings are summarized. The stochastic variation of two different input parameters has been considered, namely, torsional natural frequency and the structural nonlinear stiffness. Lognormal distribution for both the input variations is assumed. The mean values and the variance of the rotational frequency is considered in such a way that we can focus on the linear aerodynamic regime and the nonlinear dynamic stall regime separately. It has been observed that Arbitrary Polynomial Chaos expansion captures the system response well in the linear aerodynamic range. Good statistical convergence is obtained within four random modes. The use of APC enables handing non-Gaussian uncertainties without compromising on the convergence rate. The technique is also much faster than running a large number of Monte Carlo simulations, thus, is an efficient way to model the statistical properties of the system response. For example, the CPU time consumed by a standard 1000 point MC is almost ten times of that of APC for the linear problem. In the nonlinear regime, APC gives fairly good convergence but not for very large time intervals. The time degeneracy is delayed as the order of polynomial expansion increases. A similar trend is mentioned in [40,39], where they observe oscillatory decay at large times instead of limit cycle oscillations which occurs as a result of energy loss. A possible remedy for this problem would be by using Fourier basis functions [42] or a

wavelet based approach [39], instead of Gram–Schmidt polynomials.

7. Concluding remarks

An algorithm for capturing the propagation of uncertainties on a dynamic stall flutter system has been presented. The uncertainties are represented by using Arbitrary Polynomial Chaos. An appropriate polynomial chaos basis is constructed within the arbitrary polynomial chaos framework using the statistical moments of the uncertain input in a Gram–Schmidt orthogonalization. The arbitrary polynomial chaos results have been compared with those obtained from Monte Carlo simulations. The system is seen to be sensitive to uncertainties in the input parameters considered here, as shown in the bifurcation diagrams. The use of APC enables one to obtain accurate results for damped oscillation at computational costs of less than one-tenth to that of Monte Carlo simulations. For limit cycle oscillations, the accuracy of the polynomial chaos approximation decreases with time, which is equivalent to what has been found in previous studies. Also, in this special case of the viscous nonlinear terms in the dynamic stall model, the computational time for the numerical integration increases significantly for oscillations above the stall angle. In a separate study, a nonintrusive polynomial chaos approach will be applied in order to overcome this problem. It is to be noted that the present study is a numerical investigation of the APC technique as applied to an uncertain stall flutter system. Further studies are currently being undertaken to use this method for quantifying the uncertainties in predicting the instability boundaries in details.

References

[1] Chaviaropoulos P. Flap/lead-lag aeroelastic stability of wind turbine blade sections. Wind Energy 1999;2:99–112.

[2] Chaviaropoulos P et al. Viscous and aeroelastic effects on wind turbine blades. the VISCEL project. Part II: aeroelastic stability investigations. Wind Energy 2003;6:387–403.

[3] Dowell E, Curtiss HJ, Scanlan R, Sisto F. A modern course in aeroelasticity. Dordrecht: Kluwer Academic Publisher; 1989.

[4] Fung Y. An introduction to the theory of aeroelasticity. New York: John Wiley & Sons, Inc; 1955.

[5] Alighanbari H, Price S. The post-hopf bifurcation response of an airfoil in incompressible, two-dimensional flow. Nonlinear Dyn 1996;10(4):381–400.

[6] Tang D, Dowell E. Comparison of theory and experiment for nonlinear flutter and stall response of a helicopter blade. J Sound Vib 1993;165(2):251–76.

[7] Tang D, Dowell E. Nonlinear aeroelasticity in rotorcraft. Math Comput Model 1993;18:157–84.

[8] Lee B, Price S, Wong Y. Nonlinear aeroelastic analysis of airfoils: bifurcation and chaos. Prog Aerospace Sci 1999;35:205–334.

[9] Sheta E, Harrand V, Thompson D, Strganac TW. Computational and experimental investigation of limit cycle oscillations of nonlinear aeroelastic systems. J Aircraft 2002;39(1):133–41.

[10] Fragiskatos G. Nonlinear response and instabilities of a two-degree-of-freedom airfoil oscillating in dynamic stall. M Eng Masters thesis, McGill University; 1999.

[11] Lee B, Tron A. Effects of structural nonlinearities on flutter characteristics of the cf-18 aircraft. J Aircraft 1989;26(8):781–6.

[12] Dowell E, Edwards J, Strganac T. Nonlinear aeroelasticity. J Aircraft 2003;40(5):857–74.

[13] O'Neil T, Strganac T. Aeroelastic response of a rigid wing supported by nonlinear springs. J Aircraft 1998;35(4):616–22.

[14] Bathe K. Finite element procedures. New Jersey: Prentice Hall; 1996.

[15] Peters D. Towards a unified lift model for use in rotor blade stability analyses. J Am Helicopter Soc 1985;30:32–42.

[16] Tran C, Petot T. Semi-empirical model for the dynamic stall of airfoils in view of the application to the calculation of responses of a helicopter blade in forward flight. Vertica 1981;5:35–53.

[17] Dunn P, Dugundji J. Nonlinear stall flutter and divergence analysis of cantilevered graphite/epoxy wings. AIAA J 1992;30(1):153–62.

[18] Beedy J, Barakos G, Badcock K, Richards B. Nonlinear analysis of stall flutter based on the Onera aerodynamic model. Aeronaut J 2003;107(1074):495–509.

[19] Sarkar S, Bijl H. Stall induced vibration and flutter in a symmetric airfoil. In: Proceeding of ASME pressure vessel and piping division conference, 6th international symposium on fluid structure interaction, aeroelasticity, flow induced vibrations and noise, Vancouver, Canada; 2006.

[20] Kleiber M, Hien T. The stochastic finite element method. New York: John Wiley and Sons; 1992.

[21] Ghanem R, Spanos P. Stochastic finite elements: a spectral approach. New York: Springer-Verlag; 1991.

[22] Wiener N. The homogeneous chaos. Am J Math 1938;60:897–936.

[23] Wiener N. Nonlinear problems in random theory. New York: MIT Technology Press and John Wiley and Sons; 1958.

[24] Cameron R, Martin W. The orthogonal development of nonlinear functionals in series of Fourier–Hermite functionals. Ann Math 1947;48:385–92.

[25] Ghanem R. Stochastic finite elements with multiple random non-Gaussian properties. J Eng Mech 1999;125:26–40.

[26] Xiu D, Karniadakis G. The Wiener–Askey polynomial chaos for stochastic differential equations. SIAM J Sci Comput 2002;24(2):619–44.

[27] Wan X, Karniadakis G. Beyond Wiener–Askey expansions: handling arbitrary pdfs. J Sci Comput 2006;27:455–64.

[28] Xiu D, Lucor D, Su C-H, Karniadakis G. Stochastic modeling of flow-structure iterations using generalized polynomial chaos. J Fluid Eng 2002;124:51–9.

[29] Xiu D, Karniadakis G. Modeling uncertainty in flow simulations via generalized polynomial chaos. J Comput Phys 2003;187:137–67.

[30] Wan X, Karniadakis G. An adaptive multi-element generalized polynomial chaos method for stochastic differential equations. J Comput Phys 2005;209:617–42.

[31] Wan X, Karniadakis G. Long-term behavior of polynomial chaos in stochastic flow simulations. Comput Meth Appl Mech 2006;159:5582–96.

[32] Witteveen J, Bijl H. Modeling arbitrary uncertainties using Gram–Schmidt polynomial chaos. 44th AIAA Aerospace Sciences Meeting and Exhibit, Reno, Nevada AIAA-2006-896; 2006.

[33] Nigam N, Narayanan S. Applications of random vibrations. New Delhi: Narosa Publishing House; 1994.

[34] Lind R, Brenner M. Robust flutter margin analysis that incorporates flight data, NASA/TP-1998-206543; 1998.

[35] Pettit C. Uncertainty in aeroelasticity analysis, design and testing. In: Nicolaidis E, Ghiocel D, editors. Engineering design reliability handbook. Boca Raton, FL: CRC Press; 2004.

[36] Pettit C. Uncertainty quantification in aeroelasticity: recent results and research challenges. J Aircraft 2004;41(5):1217–29.

[37] Poirin F. On some stochastic method applied to aeroservoelasticity. Aerospace Sci Technol 2000;4:201–14.

[38] Borglund D. Robust aeroelastic stability analysis considering frequency-domain aerodynamic uncertainty. J Aircraft 2003;40(1):189–193.

[39] Pettit C, Beran P. Spectral and multiresolution wiener expansions of oscillatory stochastic process. J Sound Vib 2006;294:752–79.
[40] Pettit C, Beran P. Polynomial chaos expansion applied to airfoil limit cycle oscillations. In: 45th AIAA/ASME/ASCE/AHS/ASC structures, structural dynamics and materials conference, California AIAA 2004-1691; 2004.
[41] Le Maître O, Knio O, Najm H, Ghanem R. Uncertainty propagation using Wiener–Haar expansions. J Comput Phys 2004;197:28–57.
[42] Millman D, King P, Beran P. A stochastic approach for predicting bifurcation of a pitch and plung airfoil. In: 21st AIAA applied aerodynamics conference, Orlando, FL AIAA-2003-3515; 2003.
[43] Pettit C, Gandhi R. Optimization of a wing structure for gust response and aileron effectiveness. J Aircraft 2003;40(6):1185–91.
[44] Liaw D, Yang H. Reliability and nonlinear supersonic flutter of uncertain laminated plates. AIAA J 1993;31(12):2304–11.
[45] Ibrahim R, Beloiu D, Pettit C. Influence of joint relaxation on deterministic and stochastic panel flutter. AIAA J 2005;43(7): 1444–1454.
[46] Choi S, Namachchivaya N. Stochastic dynamics of a nonlinear aeroelastic system. AIAA J 2006;44(9):1921–31.
[47] Lindsley N, Beran P, Pettit C. Effects of uncertainty on nonlinear plate aeroelastic response. In: 43rd AIAA/ASME/ASCE/AHS/ASC structures, structural dynamics, and materials conference, Denver, Colorado AIAA 2002-1271; 2002.
[48] Shubov M. Mathematical modeling and analysis of flutter in bending-torsion coupled beams, rotating blades, and hard disk drives. J Aerospace Eng 2004;17(2):56–69.
[49] Shubov M. Flutter phenomenon in aeroelasticity and its mathematical analysis. J Aerospace Eng 2006;19(1):1–12.
[50] Gautschi W. Orthogonal polynomials; computation and approximation. Oxford: Oxford University Press; 2004.
[51] Golub G, Van Loan C. Matrix computations. 3rd ed. Baltimore, MD: John Hopkins University Press; 1996.
[52] Migliore P, Cheney M. Feasibility study of pultruded blades for wind turbine rotors, AIAA-2000-0061; 2000.
[53] Stiesdal H. The wind turbine components and operation. Bonus-Info, Newsletter; 1999.
[54] Hou T, Wuan L, Rozovskii B, Zhou H-M. Wiener chaos expansions and numerical solutions of randomly forced equations of fluid mechanics. J Comput Phys 2006;216:687–706.